JOURNAL OF GEOPHYSICAL RESEARCH, VOL. 95, NO. C5, PAGES 7155–7166, MAY 15, 1990

The Northeast Pacific Ocean Response to the 1982–1983 El Niño

MARK A. JOHNSON AND JAMES J. O'BRIEN

Mesoscale Air-Sea Interaction Group, Florida State University, Tallahassee

The ocean's response to atmospheric forcing and to forcing along the coast by Kelvin waves is examined in light of nearshore seasonal variability and the major 1982–1983 El Niño. In addition to driving the northeast Pacific gyre and local currents, the wind modifies the depth to the main thermocline, changing the apparent westward phase speed of Rossby waves excited by passing Kelvin waves. The amplitude of the passing Kelvin wave determines whether the Rossby wave depresses or raises the thermocline while propagating westward. Along the northeast Pacific coast from Oregon to Washington, model results suggest that the wind raises the main thermocline during the 1982–1983 El Niño. Generally, the coastal response off Oregon and Washington appears to be strongly driven by the large-scale atmosphere, while along the California coast and south to the equator, the dominant El Niño signal has an oceanic origin. That signal, with periods between 2 and 5 years, originates in the western equatorial Pacific Ocean and is tracked eastward through the equatorial waveguide and then poleward along the coast to 50°N using data from two reduced gravity, primitive equation models coupled at 18°N. At shorter, seasonal time scales, the acceleration of the wind appears to be an important mechanism in driving coastal currents.

INTRODUCTION

A major El Niño event occurred in the equatorial and tropical Pacific Ocean during late 1982 and early 1983. Evidence for other major El Niño events dating back to 1525 has been found in the historical record by *Quinn et al.* [1987]. However, the cause of El Niño and its effects at higher latitudes is subject to debate. The response of the mid-latitude ocean to atmospheric forcing and to propagating oceanographic events originating in the equatorial Pacific is the focus of this paper. *Pares-Sierra and O'Brien* [1989] first compared the modeled response of the northeast Pacific Ocean due to atmospheric forcing with the modeled response due to oceanic forcing in the form of Kelvin waves along the Pacific coast for the years 1961 through 1979. In this paper we extend the model results through 1984 and track coastal signals to their source in the equatorial Pacific Ocean. We focus on forcing of the 1982–1983 El Niño and seasonal variations of nearshore currents.

At the annual period the oceanic signal in the northeastern Pacific was attributed to large-scale wind forcing (i.e., greater than 1000 km) by *Halliwell and Allen* [1984]. Their comparison between the ocean's response, as indicated by sea level variance, and different directions of propagating atmospheric disturbances showed a stronger response to atmospheric events with poleward motion than to events with equatorward motion. At longer periods, other mechanisms in addition to atmospheric forcing were shown to be important.

To explain observations of sea level variability off the coast of Oregon, *Clarke* [1977] invoked both free and forced waves as solutions to the linear, wind-forced, quasi-geostrophic equations. These waves contributed to the variability along the west coast at the forcing period [*Gill and Schumann*, 1974]. At periods between 2 and 5 years, *Pares-Sierra and O'Brien* [1989] identified a major source of sea level variability along the coast of North America as poleward propagating baroclinic Kelvin waves. Studies focusing on periods longer than 1 year [*Simpson*, 1984; *Norton et al.*, 1985; *Huyer and Smith*, 1985; *Rienecker and Mooers*, 1986; *Inoue et al.*, 1987; *Inoue and O'Brien*, 1987] show the importance of both the atmosphere and the ocean to variability over a range of periods.

The comparative strengths of forcing by the atmosphere and by the ocean are the basis for two hypotheses that explain large-scale ocean variability in the northeast Pacific. These hypotheses, discussed by *Emery and Hamilton* [1985], explain how El Niño is triggered and subsequently modifies the tropical and mid-latitude Pacific Ocean. Although some authors may disagree with our catagorizing their work, Table 1 attempts to identify the causes of oceanic variability associated with El Niño and, at least, shows that El Niño forcing is incompletely understood.

The atmospheric teleconnection, first suggested by *Bjerknes* [1966], requires a dynamic link between the atmosphere and the ocean and is supported by both observation and theoretical studies [*Emery and Hamilton*, 1985]. The atmospheric teleconnection links the tropical to the mid-latitude Pacific Ocean via the atmospheric Hadley cell. Cold sea surface temperature (SST) anomalies in the subtropical Pacific Ocean produce an atmospheric downdraft that reduces the Hadley circulation [*Huang*, 1978].

McCreary and Anderson [1984] showed that Walker circulation becomes active when the eastern Pacific basin is cool. When Walker circulation is active, equatorial Kelvin waves are excited, and propagating eastward, they eventually reflect at the eastern boundary as Rossby waves. After several months, these westward propagating Rossby waves reflect at the western boundary as Kelvin waves. Propagating eastward, they allow the basin to return to equilibrium. They also carry information poleward along the coast.

Rienecker and Mooers [1986] related the anomalous atmospheric circulation in the northeast Pacific to unusual conditions along the west coast of North America during the 1982–1983 El Niño. They also suggested that temperature anomalies along the west coast may be related to northward propagating coastally trapped waves. Poleward propagation of information is central to the oceanic teleconnection hypothesis. *Huyer and Smith* [1985] used conductivity-

Paper number 89JC03614.
0148-0227/90/89JC-03614$05.00

TABLE 1. Previous Studies of El Niño Forcing

Authors		Oceanic	Atmospheric
Weare et al. [1976]	EOFs of SST data, 1949–1973		
Enfield and Allen [1980]	correlations of SST and SSH anomalies	x	
Chelton and Davis [1982]	EOFs of monthly tide gauge data	x	
Rasmussen and Carpenter [1982]	cross-spectral analysis of satellite data and surface and ship observations		
Rasmussen and Wallace [1983]	observational data and inferences from atmosphere general circulation models		
Pan and Oort [1983]	correlations of 15 years (1958–1973) of ship and rawinsonde data		
Simpson [1983, 1984]	scale analysis of subsurface ship data		
Emery and Hamilton [1985]	correlations of SST and SSH along coastal British Columbia from meteorological and oceanographic data		
Huyer and Smith [1985]	CTD measurement off Oregon		
Wyrtki [1985*a*]	mapping and sea level data		
Rienecker and Mooers [1986]	SST and atmospheric data	x	
Lagos et al. [1987]	SST along equatorial Pacific and coastal Peru	x	

The authors listed at left have examined El Niño and/or the mid-latitude El Niño. Their data and methods (described in the middle column) give support to the oceanic or atmospheric teleconnection hypothesis as a forcing mechanism in the mid-latitudes. EOF, empirical orthogonal function; SST, sea surface temperature; SSH, sea surface height; CTD, conductivity-temperature-depth.

temperature-depth (CTD) and moored instrument data to conclude that the first signal of the 1982–1983 El Niño arrived by an oceanic path but that local forcing by the atmosphere reinforced El Niño conditions off the coasts of Oregon and Washington.

An oceanic teleconnection requires that the ocean carry information from the equatorial Pacific eastward in the equatorial waveguide and then poleward along coastal North and South America. In support, *Moore* [1968], and later *Clarke* [1983], established that eastward propagating disturbances, upon reflection at the equatorial eastern boundary, excite poleward propagating disturbances. Using *Clarke*'s [1983] remote wind forced coastally trapped wave theory, *Battisti and Hickey* [1984] found high coherence squared between observed alongshore velocity and the predicted subsurface pressure along the Oregon and Washington coasts. During the summers of 1972 and 1978, the region of remote forcing was located between San Francisco and Cape Mendocino, California.

A poleward propagating signal was shown to be coherent over scales of several thousand kilometers by *Spillane et al.* [1987] using hourly sea level observations along the west coast of North and South America. When coherence between coastal sea level events and the local atmospheric pressure, the wind-stress, and the wind stress curl was found to be poor, remote forcing from the equatorial Pacific waveguide was suggested.

These observations illustrate possible effects of atmospheric driving and propagating ocean waves. To examine the role of the atmosphere and of remote ocean signals in driving variability along coastal America, we utilize two existing numerical models of the equatorial and northeast Pacific Ocean. These models are well documented and reproduce many of the observed upper layer features of the large-scale ocean [*Inoue and O'Brien*, 1987; *Kubota and O'Brien*, 1988; *Pares-Sierra and O'Brien*, 1989].

In the next section, a discussion of the models is presented. The following section presents model data in support of the oceanic pathway for the mid-latitude El Niño. Comparisons between model results and observational data are also presented. The conclusions follow.

2. NUMERICAL MODELS

The results presented in this paper depend upon two primitive equation transport models of the equatorial and northeast Pacific Ocean. The equatorial Pacific model is linear and includes the entire west-east extent of the Pacific Ocean from from 20°S to 25°N. A second model of the northeast Pacific is nonlinear and extends from 18°N to 50°N from the west coast of North America to 155°W, the longitude of Hawaii. Neither model includes topographic effects. Figure 1 shows both model domains. The models are in spherical coordinates with ϕ (longitude) increasing toward the east and θ (latitude) increasing toward the north.

The model equations are

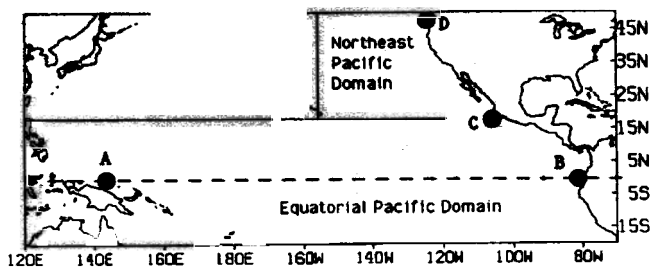

Fig. 1. The equatorial Pacific model domain and the northeast Pacific model domain. Solutions from the equatorial Pacific model are used to force the northeast Pacific model along the gap near point C. Model data are extracted along the data line AB and along the coast (line BCD) and at latitudes 25°N, 35°N, and 45°N.

$$\frac{\partial U}{\partial t}+\frac{1}{a\cos\theta}\frac{\partial}{\partial\phi}\left(\frac{U^2}{H}\right)+\frac{1}{a}\frac{\partial}{\partial\theta}\left(\frac{UV}{H}\right)-(2\Omega\sin\theta)V$$

$$=\frac{-g'}{2a\cos\theta}\frac{\partial H^2}{\partial\phi}+\frac{\tau^{\phi}}{\rho}+A\nabla^2U \qquad (1)$$

$$\frac{\partial V}{\partial t}+\frac{1}{a\cos\theta}\frac{\partial}{\partial\phi}\left(\frac{UV}{H}\right)+\frac{1}{a}\frac{\partial}{\partial\theta}\left(\frac{V^2}{H}\right)+(2\Omega\sin\theta)U$$

$$\frac{-g'}{2a}\frac{\partial H^2}{\partial\theta}\quad\rho+A\nabla^2V \qquad (2)$$

$$\frac{\partial H}{\partial t}+\frac{1}{a\cos\theta}\left\{\frac{\partial U}{\partial\phi}+\frac{\partial}{\partial\theta}(V\cos\theta)\right\}=0 \qquad (3)$$

The variables U and V are transport in the east and north directions, H is the depth of the upper layer, g' is the reduced gravity, equal to $g(\Delta\rho/\rho)$, τ^{θ} and τ^{ϕ} are the wind stresses applied as a body force over the upper layer, A is an eddy viscosity coefficient, a is the radius of the Earth, and Ω is the Earth's rotation rate.

The equatorial Pacific ocean model adopts an initial upper layer depth (H) of 300 m, and the northeast Pacific model uses 200 m. The upper layer depth defines the phase speed of the waves in the model. Both models use a C grid. The equatorial model uses spacing between like variables of one quarter of a degree and the northeast Pacific model uses one sixth of a degree spacing. The finer resolution in the northern model is needed because of the smaller Rossby radius at higher latitudes. Additional details are presented for the equatorial Pacific model by *Kubota and O'Brien* [1988] and for the northeast Pacific model by *Pares-Sierra and O'Brien* [1989].

Monthly averages of the observed wind stresses (from ship of opportunity) drive the equatorial Pacific model. The northeast Pacific model is forced by the monthly averaged wind stresses from the Comprehensive Ocean Atmosphere Data Set (COADS). These winds are derived mainly from ship of opportunity data and are averaged over 2° × 2° latitude-longitude boxes. For use in the model, the observed winds are Hanning smoothed ($\frac{1}{4}-\frac{1}{2}-\frac{1}{4}$ weighting), once each in the zonal and meridional directions. The wind stress values are then interpolated to the model resolution.

To explore the effect of the equatorial Pacific on the mid-latitude ocean, the solutions from the equatorial model force the southern boundary of the northeast Pacific model from the coast westward 1600 km. This form of coupling allows the equatorial Pacific model solution to drive the northeast Pacific model. The 1600-km connection is long, and we expect that it could be reduced. The original hypothesis was that coastal Kelvin waves propagating from the equatorial model poleward to the mid-latitudes influenced the oceanography in the northeast Pacific. To insure that all the information near the coast passed into the northern model, an open connection of 15° (1600 km) was specified. In retrospect, we believe that the length could be reduced to a few degrees (several hundred kilometers) without altering the results discussed in this paper.

To isolate the influence of the equatorial Pacific solutions from those forced by the local wind stresses in the northeast Pacific model, three sets of simulations have been completed for 1975 through 1984. All three experiments were originally spun up from rest using climatological winds and then integrated from 1961 through 1975. In case I the northeast Pacific model is driven by the local wind stresses only. In case II the solution from the equatorial Pacific model alone is used to drive the northeast Pacific model. Case III uses both methods of forcing simultaneously. Figure 2 is from case III simulations and shows contours of the model upper layer thickness (ULT) off the coast of North America. ULT is an analog variable of the depth of the main thermocline and often corresponds to the sea surface temperature. Although this general relation between ULT and SST has exceptions, it is generally true in the context of this paper [see *Wyrtki*, 1985*b*].

For the results in this paper, we made some modifications to the original numerical code and corrected some minor errors in the northeast Pacific model of *Pares-Sierra and O'Brien* [1989]. In addition to the code modifications, the drag coefficient was increased to 1.5 because the frequency response function between the wind-forced model and observations showed a weak ocean response. With these changes, the simulations between 1975 and 1979 were rerun, and then the model simulations were extended through 1984.

3. RESULTS

Figure 2*a* shows contours of ULT from January 15, 1982, revealing a tongue of thin surface water (values less than 200 are shaded and indicate a shallow thermocline) extending along most of the west coast of North America as far south as 30°N, with a filament extending to 25°N. Except for the filament, this is typical of the model results during non–El Niño years. In contrast, Figure 2*b* shows ULT 1 year later during the 1982–1983 El Niño. The thin tongue (shaded) is now confined to the northwest, having been displaced poleward and offshore compared to the previous year. Thicker ULT (greater than 200 m) now occupies the coastal region along North America to the northern boundary of the model. The Pacific Gyre is also warmer, as is indicated by the thicker ULT values (see the 350-m contour line) in the central Pacific.

In this figure, currents are nearly geostrophic and generally follow contour lines. An eastward turning of the current (parallel to the 200-m contour line that contains the shaded area) near 30°N is evident in both frames of Figure 2. This shoreward bend has been discussed before [*Reid et al.*, 1963] and is claimed to be a permanent feature of the California Current system [*Hickey*, 1979]. It is always present in our model results, although its southern extent shows year-to-year variability.

The source of the El Niño signal is traced to the western equatorial Pacific Ocean. The data are from both the equatorial and northeast Pacific models along the data line ABCD shown in Figure 1. The data line extends along the equator from point A in the west to point B at the coast of Central America, and continues poleward along the coast through point C and northward to point D at the northern limit of the northeast Pacific model (50°N). The distance from point A to point D is approximately 27,000 km. Data extracted from the northeast Pacific model are from case II simulations forced at the boundary by solutions of the equatorial Pacific model.

Values of ULT from both models have been extracted along the data line and are plotted in Figure 3. The mean (computed separately for each model) has been removed,

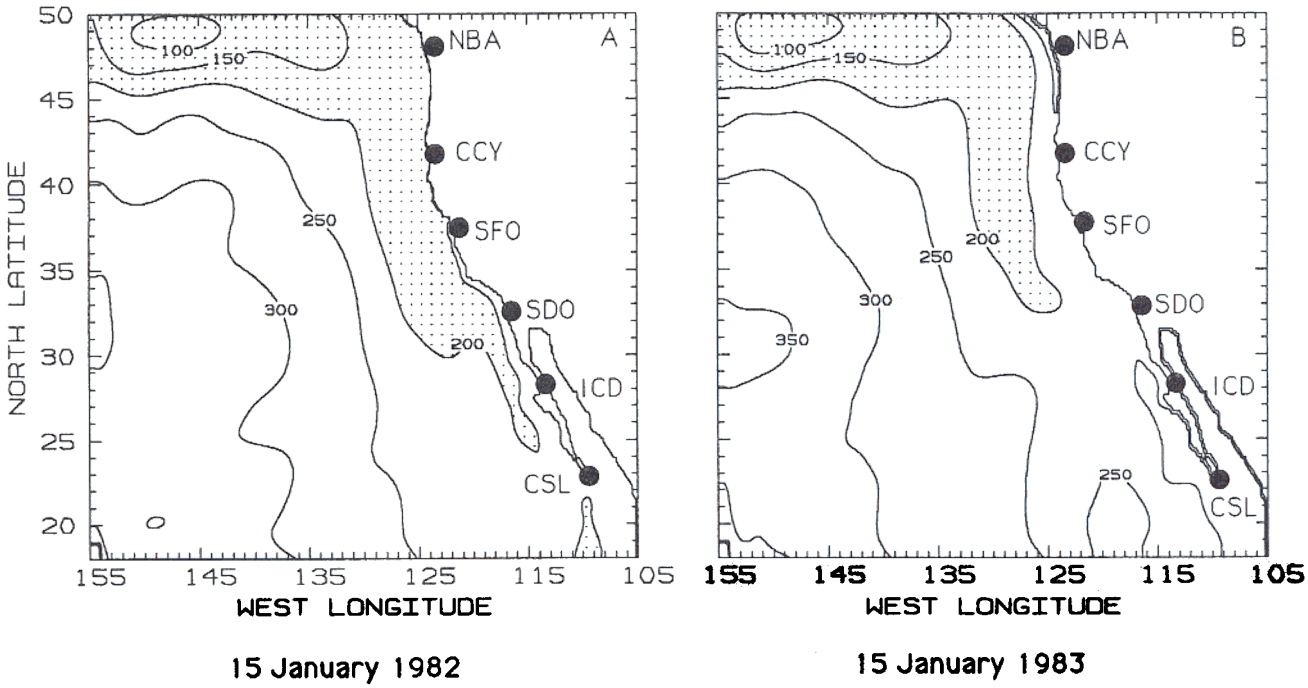

Fig. 2. Model solutions from wind and boundary forcing for (*a*) January 15, 1982, and (*b*) January 15, 1983. During 1982 a tongue of thin ULT (shaded), corresponding to cool surface water, extends equatorward to 25°N. In contrast, during the 1982–1983 El Niño (right), the thin tongue is poleward and offshore. City codes shown here also appear in later figures. They are: NBA, Neah Bay (48.4°N); CCY, Crescent City (41.8°N); SFO, San Francisco (37.8°N); SDO, San Diego (32.7°N); ICD, Islas Cedro (28.2°N); and CSL, Cabo San Lucas (22.8°N).

and values of ULT greater than the mean have been shaded, highlighting the 1982–1983 El Niño. With time increasing along the ordinate, thick ULT is seen in the left frame in late 1981 (about a year before the mid-latitude El Niño) and early 1982. The signal propagates eastward along the equator at a speed of 36 cm s^{-1}.

Variability in wave speed (as indicated by variations in the zero contour line in early 1983 between points A and B) is due to local wind effects. The ULT signal propagates poleward past point B at a speed of about 200 cm s^{-1}, in reasonable agreement with the Kelvin speed in the equatorial model (245 cm s^{-1}). One can see steady propagation from point B poleward to point C and D. Offshore propagation at 35°N is shown in the right frame and is clearly related to the passing of the coastal Kelvin wave. Offshore propagation is about 2 cm s^{-1}.

Because of the dual forcing used in the northeast Pacific model, it is important to test if the model solutions are in reasonable agreement with observations. The equatorial Pacific model solutions and their relation to observations are

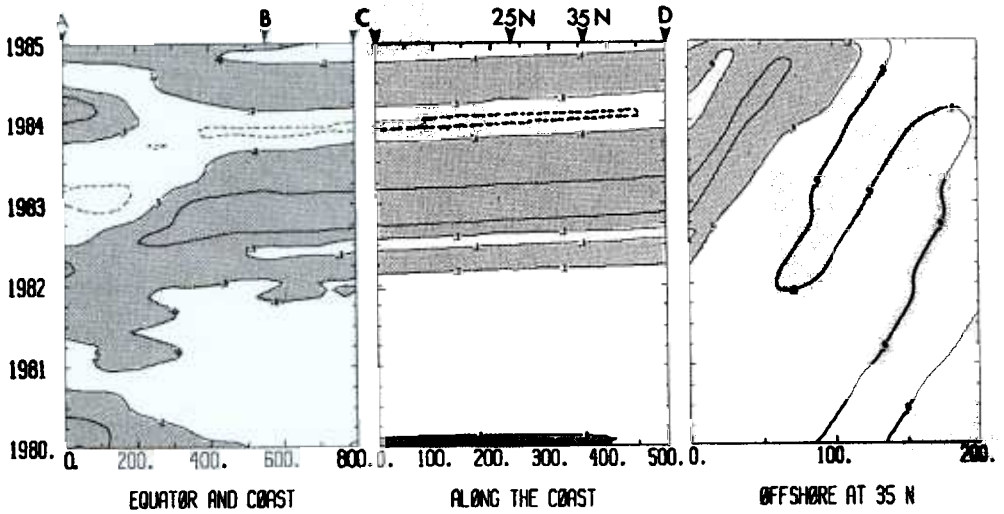

Fig. 3. The complete 1982–1983 El Niño signal. Beginning (left) in the western equatorial Pacific (point A, see Figure 1), ULT is traced eastward to the coast (point B), and then poleward to 50°N at point D (middle frame). The signal propagates offshore at 35°N (right). Contours greater than the mean are shaded. The signal requires over a year to arrive at the northeast Pacific coast at 50°N from the western equatorial Pacific.

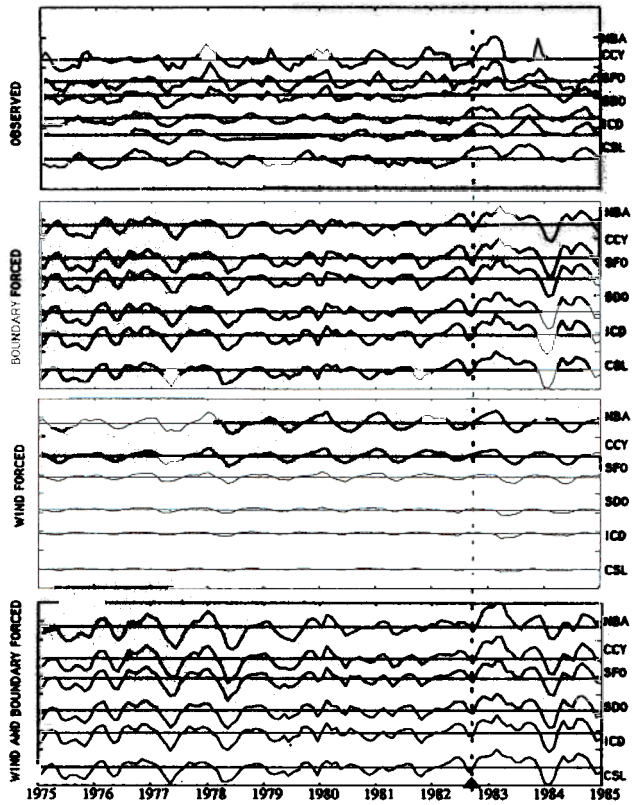

Fig. 4. Values of observed and modeled sea level for six coastal stations along the west coast of North America. Station codes and locations are shown in Figure 2. Shown from top to bottom are the observed sea level, boundary-forced sea level, wind-forced sea level, and wind- and boundary-forced sea level. The modeled sea level shows less station-to-station variability than does the observed sea level. The wind-forced sea level fluctuations weaken rapidly from north to south. The onset of the 1982–1983 El Niño in late 1982 off Oregon is marked by the dashed vertical line.

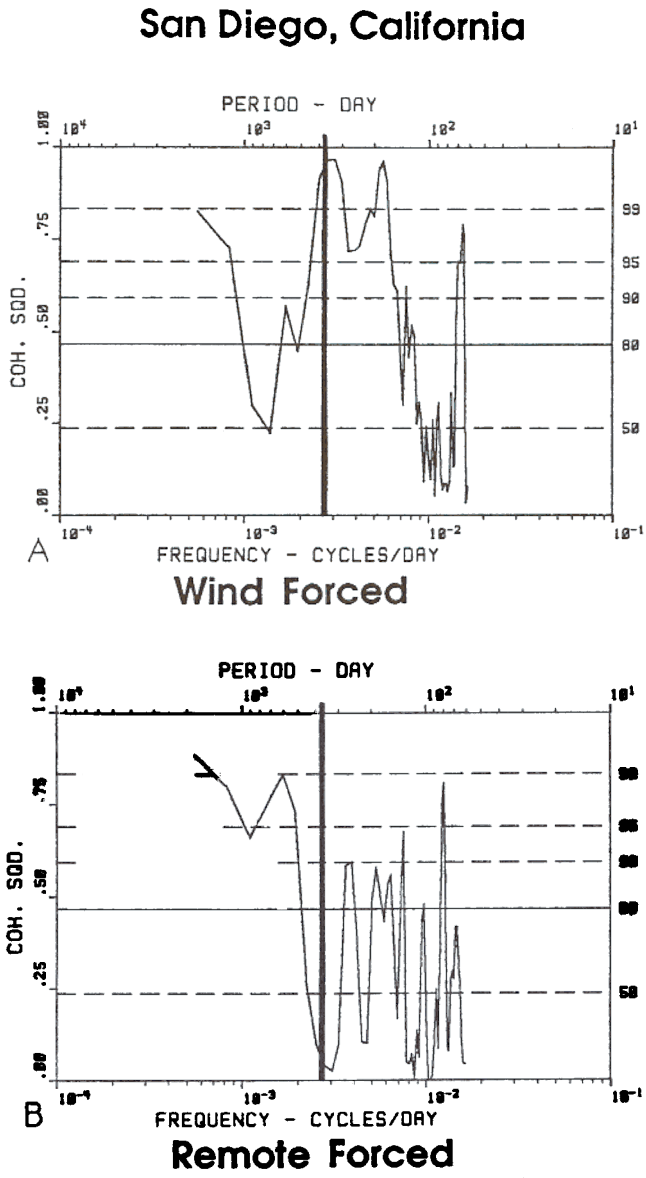

Fig. 5. Coherence squared for model and observed data from San Diego, California. Wind forcing contributes strongly to the observed signal at the annual and semiannual periods. At longer periods the remote-forced signal is the major component in the observed signal, contributing to periods where the wind-forced coherence is generally poor.

discussed by *Inoue and O'Brien* [1987] and *Kubota and O'Brien* [1988]. Comparison between observations and the northeast Pacific model results prior to 1980 shows very good agreement as well [*Pares-Sierra and O'Brien*, 1989].

Monthly means of observed sea-level were obtained from K. Wyrtki (personal communication, 1988) for all available coastal stations between 18°N and 50°N. Time series of coastal sea-level data between 1975 and 1984 are shown in the top frame of Figure 4. The lower frames show the model data from the boundary-forced, wind-forced, and wind- and boundary-forced simulations extracted from model grid points corresponding to the coastal stations. The station spacing along the vertical axis is proportional to the distance between stations.

Figure 4 shows that the model data are visually more coherent between stations than the observed data. Wind forcing alone produces weaker sea level fluctuations for the more equatorward stations, and there is no evidence for the 1982–1983 El Niño. According to observations of *Huyer and Smith* [1985], anomalously high sea level reached the Pacific northwest coast in October 1982 via an oceanic path. The observed sealevel at Neah Bay is shown at the top of Figure 4. A large increase in sea level is observed there in late 1982. The boundary forced and wind plus boundary forced results for Neah Bay also show a large-amplitude response in sealevel at the same time.

Coherence squared between model and observations have been computed; we show results at two locations only, San Diego, California, and Neah Bay, Washington, to illustrate the relation between sea level and wind or boundary forcing. The coherence squared between the observed and modeled time series at San Diego, California, is shown in Figure 5. The top frame, computed from wind-forced model data and observations, shows coherence squared above the 95% level for periods from 150 days to slightly above the annual period. The bottom frame, from the remote-forced model data and observations, shows that the signal from the equatorial Pacific contributes to annual periods and above.

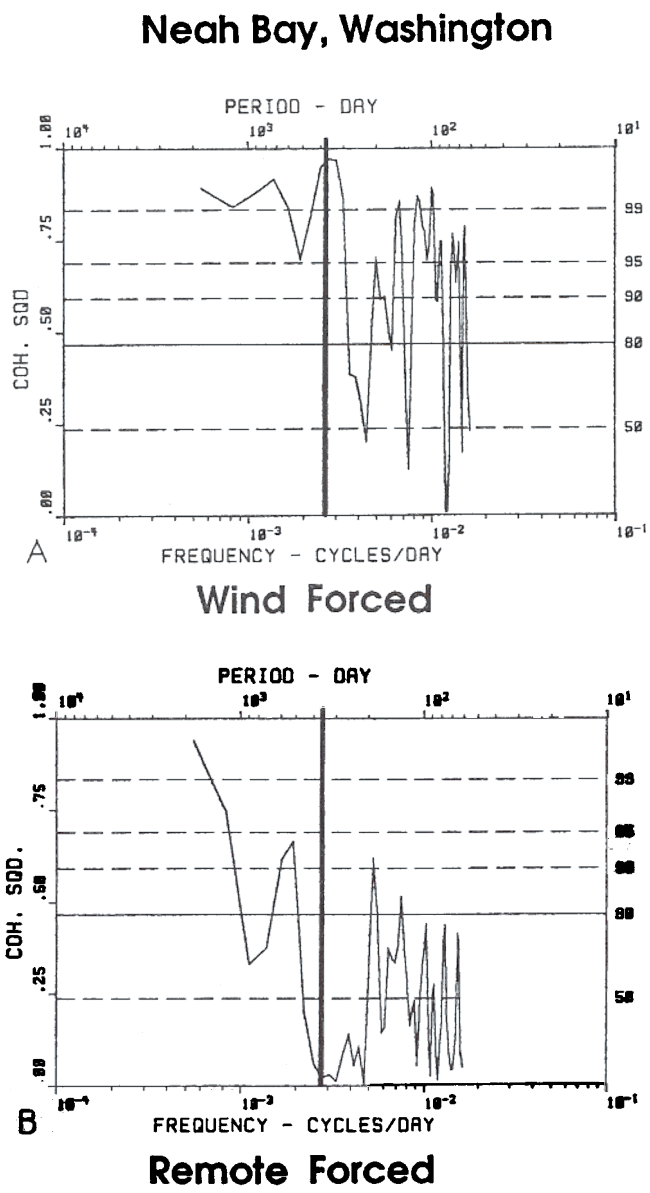

Fig. 6. Coherence squared for model and observed data from Neah Bay, Washington. In contrast to San Diego (Figure 5), the wind-forced signal contributes strongly to periods at and above the annual. The remote-forced signal contributes only at the very long periods, near the limit of this time series.

In general, the model results are generally coherent with observed sea level at San Diego.

A different result emerges from the coherence squared between modeled and observed data from Neah Bay, Washington (Figure 6). The wind-forced solution shows coherence squared above the 95% level for periods from 60 days up to 180 days. Between 200 and 300 days, the amplitude falls and then increases near the annual period and remains above the 95% level at periods above the annual. The remote-forced solution contributes to the signal only at very long periods near the resolution of the time series. Figures 5 and 6 both show that the remote signal from the equatorial Pacific influences coastal North America at interannual periods. In contrast, driving by the wind influences sea level at longer periods (interannual and above) along the northern North

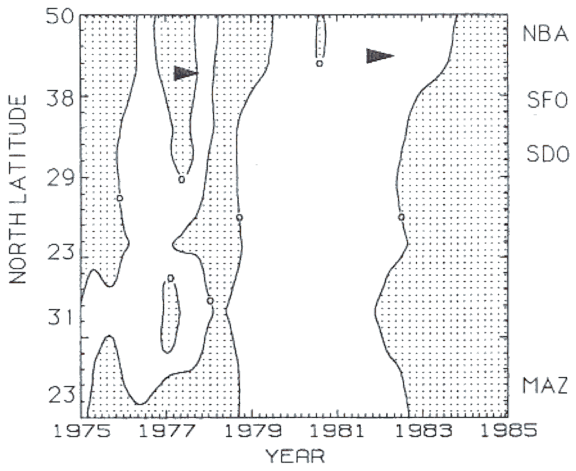

Fig. 7. Contours of coastal ULT from the wind-forced model for 1975 through 1984. Values less than the mean are shaded. Note the negative ULT values, indicating thin ULT, beginning in late 1982 and early 1983, the time of the major El Niño. The arrow indicates a region where wind stress curl thickens ULT. Station codes at right are the same as in Figure 2; MAZ is Mazatlan (23.2°N).

American coast (e.g. Neah Bay) but plays only a weak role at long periods along the southern portion of the coast (e.g. San Diego). The spectral trend between these two stations (from spectra not shown here) shows no abrupt transition in the relation between boundary and wind forcing from the northern to southern stations. There is no station where wind forcing suddenly dominates or boundary forcing suddenly weakens.

We have shown that the influence of wind forcing along the coast changes character smoothly between San Diego and Neah Bay. The wind-forced signal along the coast for 1975 through 1984 is shown in Figure 7. The spatial and temporal mean has been removed, and values less than the 10-year mean are shaded. In this and the following figures, the time axis increases along the abscissa. A thickening trend (unshaded) begins in the south and progresses northward between 1975 and 1977, the time of the 1976 El Niño. For this El Niño, atmospheric forcing appears to thicken the upper layer. Thickening begins again in 1979 and extends through late 1982. The thickening in 1979 might be construed as the beginning of an El Niño, but the anomalous conditions observed in the Pacific in 1980 were termed non-El Niño [*Quinn et al.*, 1987]. Wind-induced thickening of ULT, as seen during 1976, is absent along the coast during the period from 1982 to late 1983. Instead, the wind thins the upper layer along much of the coast, indicated by shaded ULT along coast beginning in mid to late 1982.

Thin ULT (indicative of a shallow thermocline) is expected to reduce El Niño warming. During 1982 and 1983, positive wind stress curl dominates much of the coast, with only patches of negative curl found between 23°N and 31°N (Figure 11, bottom). Near the southern boundary between 1981 and 1984, negative curl is very strong, exceeding the mean by more than 2 standard deviations. However, the region is limited and appears to have little effect in thickening ULT in the south. In the north, poleward alongshore wind stress (τ^y) is anomalously strong (see the shaded region of poleward wind stress in early 1983 in the top frame of Figure 11). The strong poleward stress reduces coastal

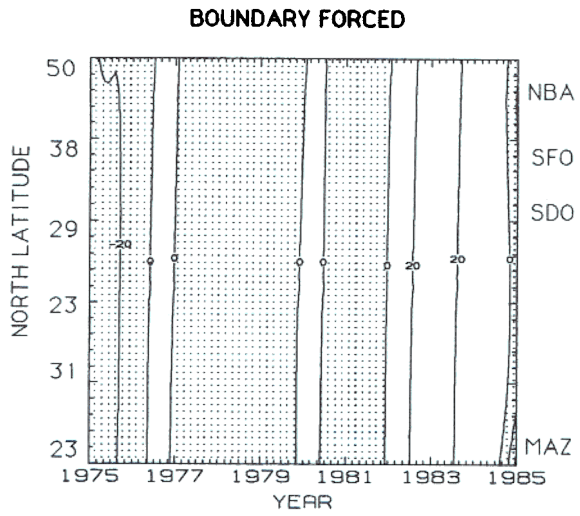

Fig. 8. Contours of coastal ULT from the boundary forced model for 1975 through 1984. Values less than the mean are shaded. Positive values corresponding to very large amplitude ULT are seen as vertical bands at the time of the 1976 and 1982–1983 El Niño. A similar band of thick ULT is seen during the time of the anomalous non–El Niño year 1980. Station codes at right are the same as in Figure 2; MAZ is Mazatlan (23.2°N).

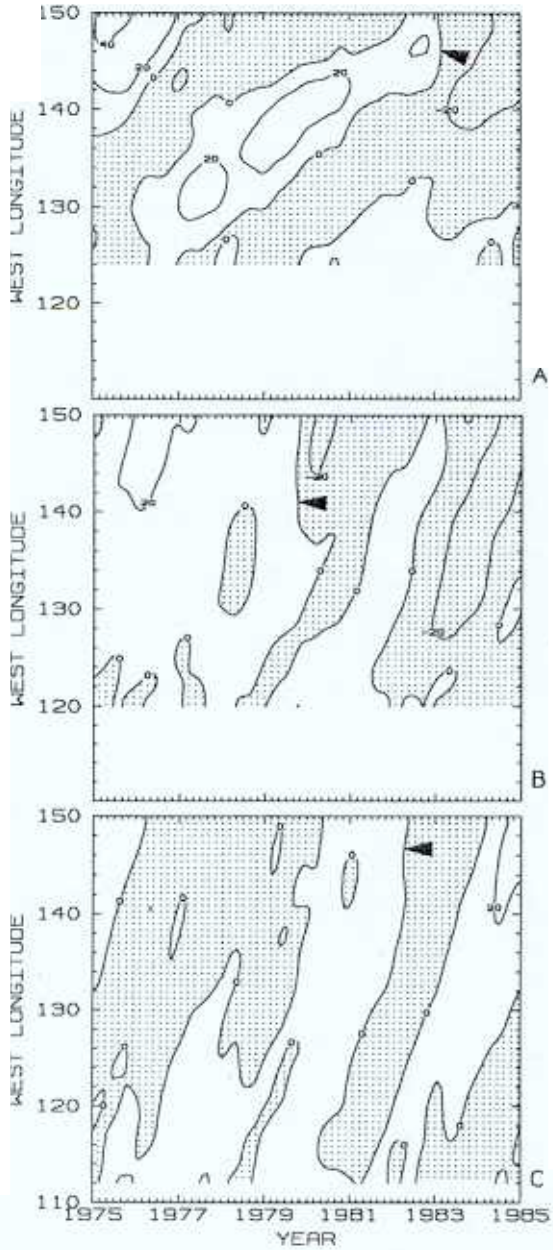

Fig. 9. Contours of ULT from the wind-forced model from the coast offshore to 150°W between 1975 and 1984. Note the difference in westward phase speed in the three frames, indicated by the changing slope of the contour lines, from (*a*) 45°N, (*b*) 35°N, and (*c*) 25°N. Regions where the local wind stress curl modifies the offshore propagation speed, indicated by arrows, show changes in the slope of the contour lines.

upwelling by pumping fluid toward the coast, maintaining thick ULT seen between 38°N and 50°N in Figure 7 in late 1982 and early 1983. In this region, atmospheric forcing strengthens the El Niño response, in agreement with *Huyer and Smith* [1985]; elsewhere, atmospheric forcing appears to weaken the El Niño response.

The northeast Pacific boundary-forced model solution from case II is shown in Figure 8. There are thick bands of ULT during late 1976, the anomalous non-El Niño year of 1980, and between 1982 and 1984. Dominating Figure 8 is the signal from the 1982–1983 El Niño. Its amplitude is larger then the signal during 1976 or 1980 by more than a factor of 2. The model results suggest that this signal accounts for the large values of sea level observed along the coast in late 1982 *Huyer and Smith* [1985]. Figure 8 shows that the 1982–1983 El Niño resulted from signals traveling along the coast. Offshore propagation initiated by the coastal ULT signal subsequently modifies ULT offshore.

Offshore propagating signals in ULT from the wind-forced model are shown in Figure 9 for the latitudes 25°N, 35°N, and 45°N. The difference in phase speed is evident among all three frames, with the phase speed (the general slope of the contour lines) decreasing from south to north. At 25°N the phase speed is 4.3 cm s^{-1}, decreasing to 2.3 cm s^{-1} at 35°N, and decreasing again to 1.1 cm s^{-1} at 45°N. These speeds are somewhat faster, but in general agreement with phase speeds of long planetary waves ($\omega/k = -\beta a^2$ [*Gill*, 1982, p. 503]). For 25°N, 35°N, and 45°N, the expected speeds are 3.4 cm s^{-1}, 1.7 cm s^{-1}, and 1.0 cm s^{-1}, respectively.

Variability in the speed of offshore propagation due to wind forcing is indicated by curved contours in Figure 9. At 25°N, a small burst of positive wind stress curl at 145°W in early 1982 (Figure 12*c*) causes thinning of ULT and an apparent slowing of the offshore speed indicated by the more vertical nature of the zero contour line at 145°W in early 1982 (Figure 9*c*). In mid-1983, negative curl extends eastward to 120°W (Figure 12*c*). This thickens ULT, causing the dip in the contour line during mid-1983 between 115°W and 120°W.

Similar wind-forced changes in ULT are visible in the other contour plots at 35°N and 45°N. For example, a burst of positive curl (greater than 2 standard deviations above the mean) in early 1980 at 35°N between 135°W and 150°W (Figure 12*b*), causes thinning at 145°W, resulting in slowing of offshore propagation (Figure 9*b*), indicated by the change in orientation of the zero contour line. At 45°N (Figure 9*a*), westward propagation of the positive ULT (at 145°W in early

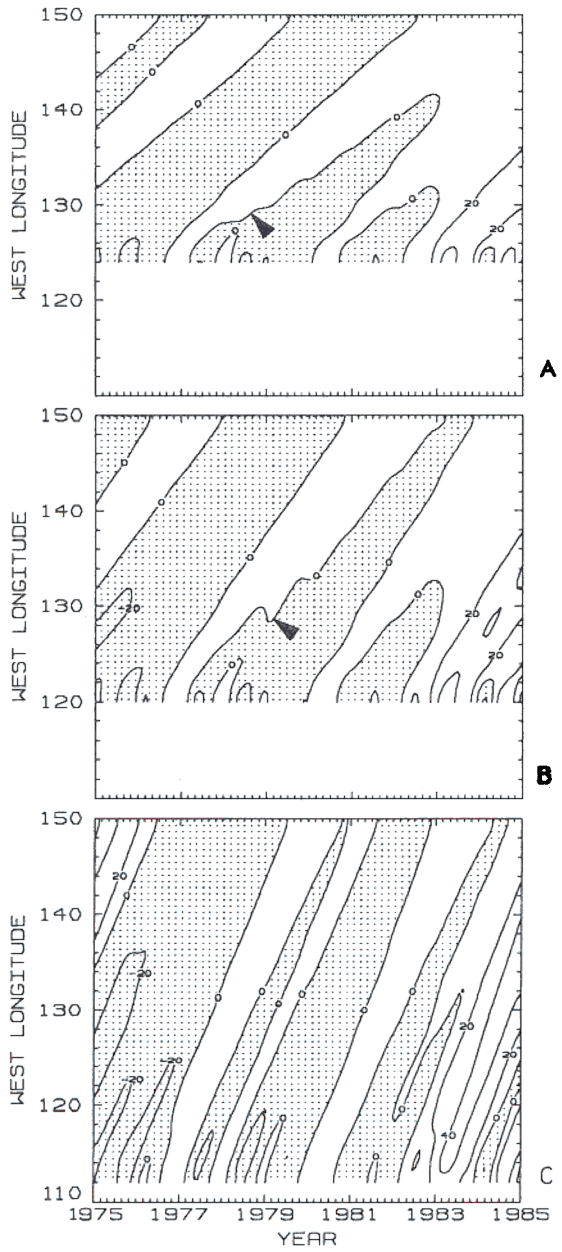

Fig. 10. Contours of ULT from the boundary-forced model between 1975 and 1984 from the coast offshore to 150°W, and at (*a*) 45°N, (*b*) 35°N, and (*c*) 25°N. Differences in offshore phase speed at these three latitudes are seen as changes in the slope of the contour lines, but without wind-induced variability.

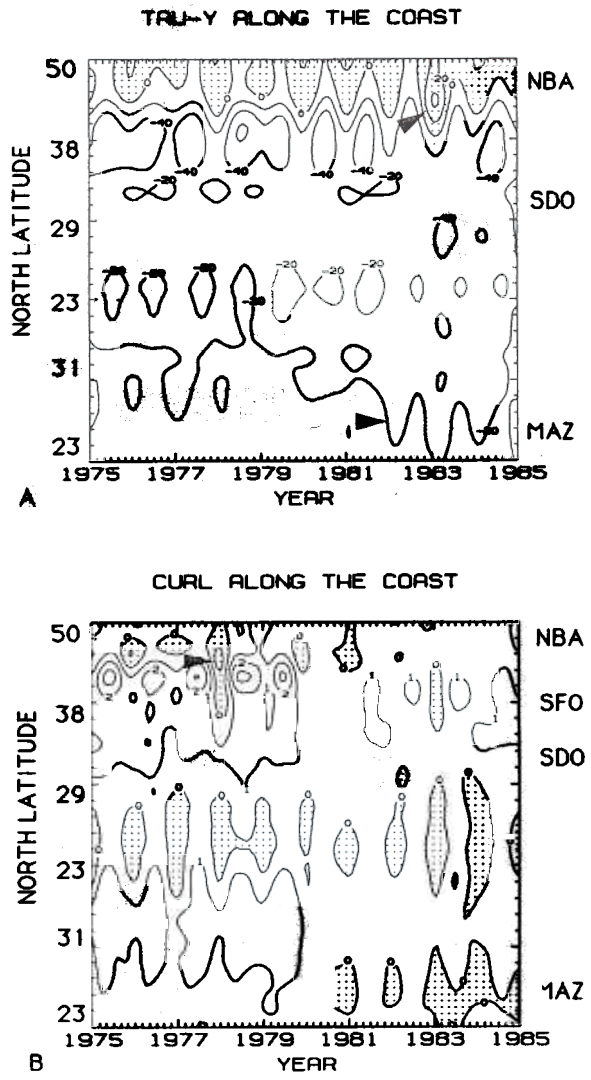

Fig. 11. (*a*) Contours of poleward wind stress along the coast. Shaded values are poleward wind stress. In the north, a region of strong poleward wind stress can be seen during late 1982 (arrow). (*b*) Contours of the wind stress curl along the coast. A strong region of negative curl is marked by the arrow in early 1978. Regions of positive curl in the Gulf of California (from 23°N to 23°N) between 1975 and 1980 contrast regions of negative curl which appear after 1980. The area of negative curl at the bottom of the frame in 1983 is unusually strong and extends to 18°N, exceeding the mean by more than 2 standard deviations. Station codes at right are the same as in Figure 2; MAZ is Mazatlan (23.2°N).

1983) is slowed and nearly halted owing to unusually large positive curl at that time (Figure 12*a*).

Without the modifying effects of the wind stress curl, offshore propagation of Rossby waves is generally constant (Figure 10). An unusual feature is the wavelike structure in the zero contour line at 130°W in early 1979 (Figure 10*b*). In early 1979, the apparent propagation speed of this feature slows and even reverses. Slowing in the offshore propagation speed is evident at 45°N along the zero contour line that originates in early 1977. We believe these changes are due to Rossby wave dispersion as it propagates westward. As the amplitude spreads out, the region of zero mean ULT is modified.

There is no simple relation between El Niño and large-scale wind stress forcing. Strong poleward pulses in wind stress are visible in Figure 11*a*. There is an especially strong burst in early 1983. Along the remaining coast, equatorward wind stress thins ULT, augmenting coastal upwelling. Along the coast, the wind stress curl (Figure 11*b*) between San Diego and Neah Bay has a strong negative pulse in early 1978. The negative pulse visibly thickens ULT (see Figure 7).

Important to alongshore propagation is a change in the character of the wind stress curl before and after 1980. Along the southern coastline before 1980, positive wind stress curl dominates to 23°N (Figure 11*b*), but after 1980, regions of negative wind stress curl are present. We expect bursts of

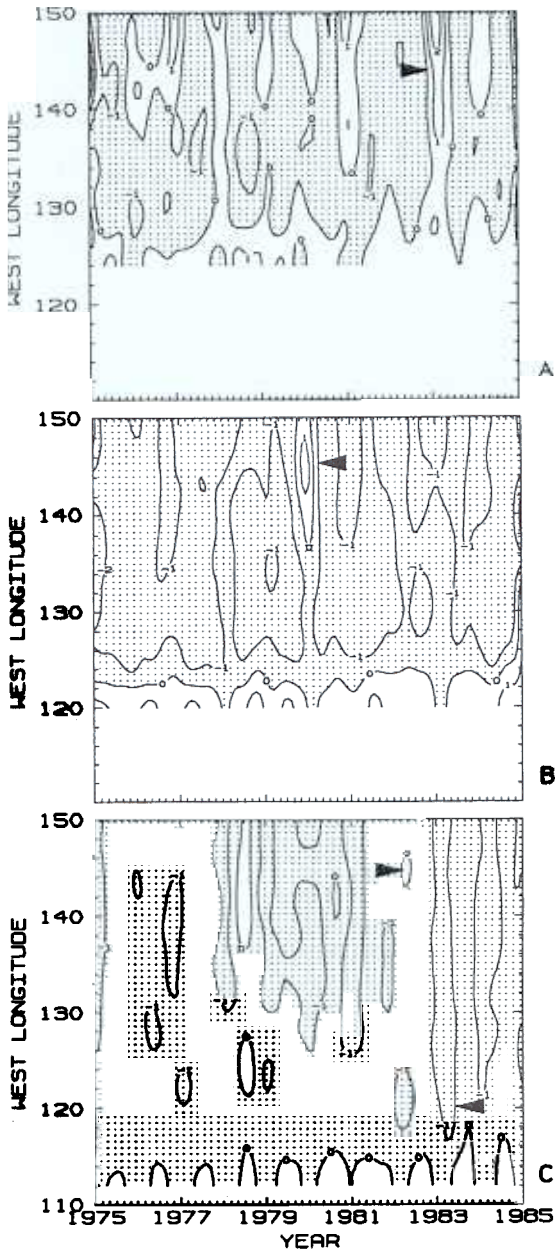

Fig. 12. Contours of wind stress curl for the latitudes (*a*) 45°N, (*b*) 35°N, and (*c*) 25°N and west to 150°W. The time-space locations that most strongly modify ULT are marked by arrows.

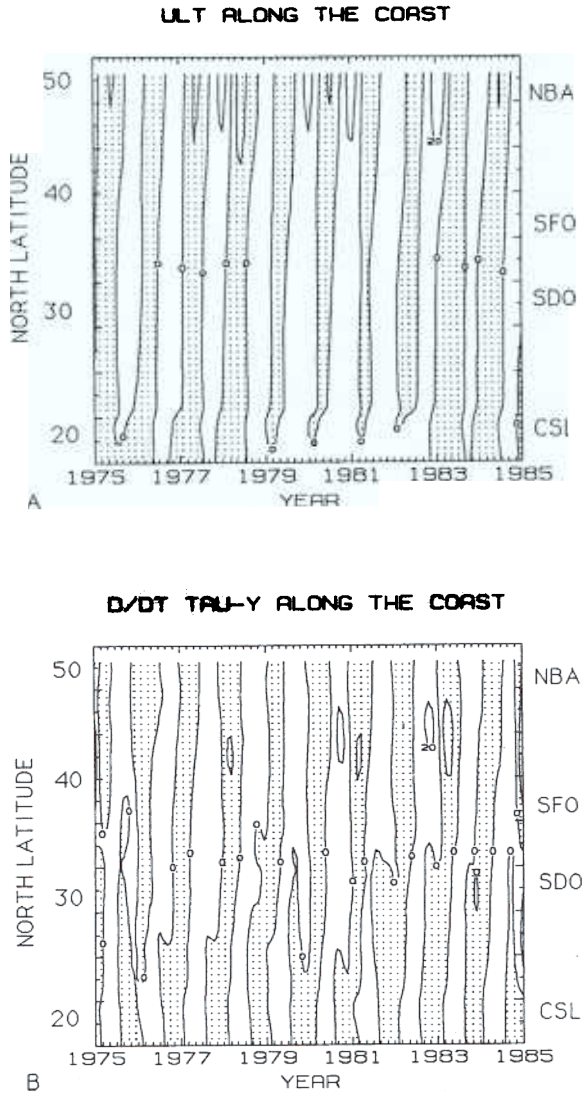

Fig. 13. (*a*) Values of ULT along the coast with the mean from each station removed. (*b*) Time derivative of the alongshore wind stress $(\partial/\partial t)\tau^y$, which appears to drive ULT poleward. Note the stalling of the large-scale wind acceleration between San Diego and San Francisco.

negative curl to thicken ULT in the south, but that is not evident in the ULT from the wind-forced model. Offshore at 25°N (Figure 12*c*), wind stress curl remains negative from 1975 through 1984 and does not indicate a characteristic change in the winds in 1980. Instead, wind stress curl at 25°N shows a region of strong negative curl penetrating shoreward during early 1983.

The coastal response, however, is related to the alongshore equatorward wind stress (Figure 11*a*), in agreement with the conclusions of *Hickey* [1979]. Strong equatorward winds extend southward during the post-1980 period and extend farthest south during 1982 and 1983. At this time, the winds thin ULT (Figure 7) along the coast and do not reinforce the El Niño response driven by the remotely forced coastal waves. At seasonal time scales, however, there is an important relation between the temporally varying wind field and the ULT along the coast.

Time variations of the wind stress curl at 25°N, 35°N, and 45°N are related to the seasonal variability of ULT along the coast. To examine this, we have removed the temporal mean of ULT along the coast at each coastal station. In Figure 13, stations along the Gulf of California have not been included in the data line along the coast, so that at 23°N the data points jump from the coast of Mexico across the gulf to the southern tip of the Baja Peninsula.

Propagation along the coast (at 40 cm s^{-1} or 35 km d^{-1}) can be seen by the slight inclination of the contour lines (Figure 13*a*). The phase speed is the same as that found by *Chelton and Davis* [1982] in 29 years of monthly mean tide gauge data along the coast of North America. The poleward propagating signal was described by Chelton and Davis as the interannual aspect of the coastal record and was related to El Niño. The interannual nature of their signal contrasts the signal from this model. For example, the model poleward

propagating ULT is seasonal, showing alternating positive and negative values. During the years between 1979 and 1983 the thin ULT (shaded) begins several hundred kilometers north of the model southern boundary.

The nature of this seasonal signal, i.e. the rapid poleward propagation, suggests that it may be Kelvin wavelike in character, although the phase speed is too slow for a first-mode Kelvin wave. We have examined the temporal change in alongshore wind stress as a possible mechanism for forcing, because it is time variations in wind stress that excite Kelvin waves. The role of seasonal variations in alongshore wind stress has been thoroughly explored by *Hickey* [1979] in a complete description of the current system offshore California. Those findings indicate that variations in alongshore wind stress are the primary driving force for the currents nearshore, but that the large-scale structure of the wind stress curl acts to damp the amplitude and modify the phase so that there are times when the current appears to lead the wind stress. Below, we examine the relation between the seasonal model ULT field along the coast and the meridional component of the wind stress for the Pacific coast from Baja to 50°N.

Figure 13*b* shows the time derivative of the alongshore wind stress, $(\partial/\partial t)\tau^y$. The alongshore wind stress is southward (except for a small region in the far north of the model), and the shaded values indicate accelerating southward winds. The character of the signal is similar to that of ULT. A difference between the character of the two signals, however, can be seen near 35°N, between San Diego and San Francisco. The poleward progression of wind acceleration stalls for 2 to 4 months before continuing poleward, and the stalling position differs from year to year. The sharp bends in the zero contour lines indicate stalling. During 1976 through 1978, the signal stalls as far south as 20°N, but in other years it stalls near 35°N. The signal stalls longest, and at its most northern position, during the 1982–1983 El Niño. At present, we cannot explain how this may effect the development of El Niño.

The correlation between the time derivative of the alongshore wind stress and ULT is shown in Figure 14 for zero, 1-month, and 2-month lags (where ULT lags $(\partial/\partial t)\tau^y$). The shaded region shows the area that is correlated above the 95% confidence limit. The stations where data were extracted are evenly distributed along the model coastline. The strongest correlation, with a value of −0.75, is seen at the left in each of the three frames. This region and the region of positive correlation to the right slowly move to the top of the frame as the lag increases, indicating that the ULT signal has moved poleward away from the region of forcing. This plot suggests that this signal is forced primarily in the southern region of the model. Otherwise, the correlation would be expected to fall along the diagonal line where the latitudes of ULT and $(\partial/\partial t)\tau^y$ are the same.

Conceptually, we believe that as the southward winds increase in strength ($(\partial/\partial t)\tau^y$ is negative), the Ekman transport offshore increases, allowing ULT to fall. Although the ULT response is rapid, it does not begin to fall below the mean value until about 1 month later, when positive correlation moves onto the diagonal. As the lag increases (from top to bottom in Figure 14), the positive correlation along the diagonal increases. After 2 months, most of the stations northward of the more northern 23°N (the region between the two 23°N is the Gulf of California) are positively correlated with the changing alongshore wind stress. Both signals (ULT and $(\partial/\partial t\tau)^y$), show slightly out of phase (about 2 months) seasonality. As the lag increases the regions of positive and negative correlation continue to move up and to the left. This transition can be seen by following the 0.25 contour line from a lag of zero months through 1 month and on to a lag of 2 months. Thus the slowly moving seasonal signal along the coast appears to be related to the seasonally changing wind stress, rather than to remotely forced El Niño events which drive coastal currents at periods from 2 to 5 years.

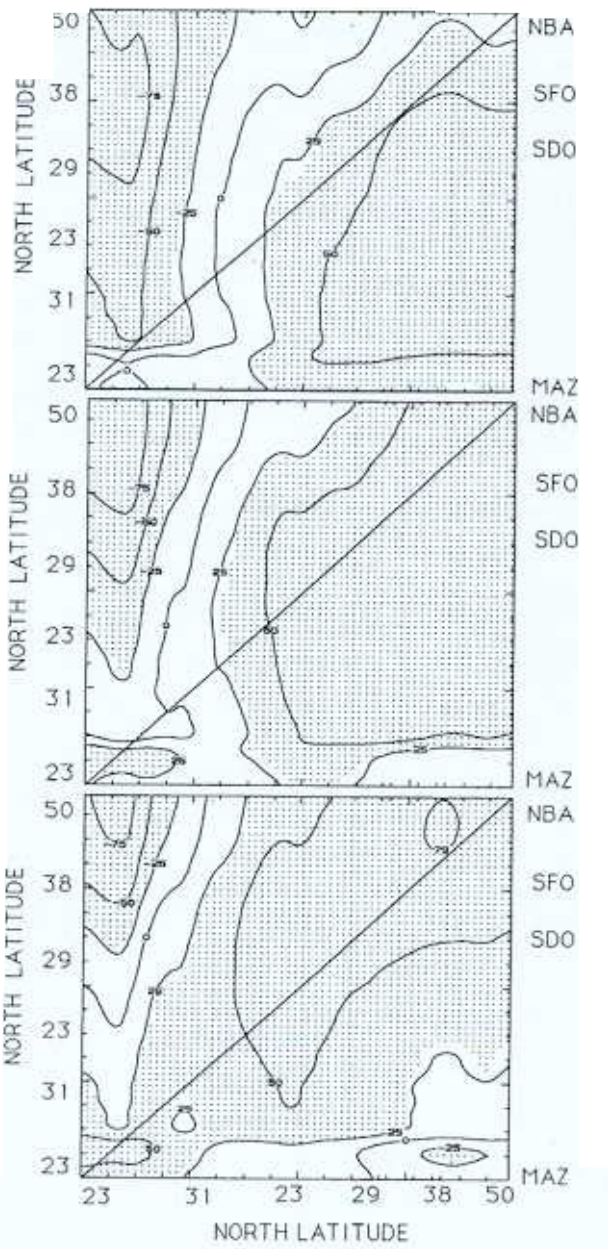

Fig. 14. Correlation between coastal station ULT and $(\partial/\partial t)\tau^y$ shown in Figure 13: (top) zero lag, (middle) 1-month lag, and (bottom) 2-month lag, with ULT lagging $(\partial/\partial t)\tau^y$. Values within the 95% confidence limit are shaded. Positive correlation progresses upward and to the left as the lag increases. Significant correlation along the diagonal from bottom left to top right would indicate that $(\partial/\partial t)\tau^y$ and ULT are correlated at each station pair. Station codes at right are the same as in Figure 2; MAZ is Mazatlan (23.2°N).

Hickey [1979] notes that off the Washington and Oregon coast (but over the continental shelf), the currents lead the wind stress. Citing the work of *Anderson and Gill* [1975], Hickey concludes that the lag difference in phase can be explained by wave theory where coastally trapped waves carry the response poleward from the region of wind stress forcing. However, there is no topography in the model presented here, so trapping by the shelf slope is not a possible explanation for our results. We suggest, then, that the phase relation may be modified by the large-scale wind stress curl at the northern latitudes.

4. CONCLUSIONS

Two primitive equation numerical models of the equatorial and northeast Pacific Ocean are used to examine the role of Kelvin waves in carrying information poleward along the coast of Central and North America and driving El Niño. The coastal Kelvin waves are the dominant factor in coastal variability at the annual and interannual periods for the mid-latitudes (i.e., El Niño), but their influence is diminished near the more northern latitudes of the model (poleward of 45°N). Coastal Kelvin waves are central to the development of the mid-latitude El Niño along the coast of North America because they excite offshore propagating Rossby waves. The coherence between the model and observed data showed that at longer periods, the ocean response at northern latitudes is more strongly related to the wind field than the response at southern latitudes.

Offshore propagation of the coastal signal modifies the central Pacific Ocean at El Niño time scales (2 to 5 years) and is directly related to wind forcing approximately 1 year earlier in the western equatorial Pacific. The pathway along the equatorial waveguide and along the coast carries the El Niño signal to the mid-latitudes. Local wind forcing modifies the offshore propagating signal. Accelerations of the alongshore wind stress are also shown to affect the seasonal sealevel along the coast. This seasonal signal propagates at 40 cm s^{-1} poleward along the coast. Seasonal accelerations of the alongshore wind stress are shown to be correlated with the ocean signal, although stalling in the poleward progression of the wind stress acceleration evident at mid-latitude, decreases the correlation in the northern latitudes. This seasonal mechanism appears to be unrelated to the formation (at longer periods) of the mid-latitude El Niño.

Acknowledgments. This research is supported by the National Science Foundation (grants 8415986 and 8811316). Both the Physical Oceanography Section and the Climate Dynamics Section contribute to the funding. Additional support was provide by the Florida State University through time granted on their Cyber 205 supercomputer. The wind stress fields are prepared under a grant from the TOGA Project Office of NOAA (grant NA84AA-D-00049). Large models require the input of many people. We thank David Legler (winds), Masa Kubota (Equatorial Model), Alejandro Pares-Sierra (Northeast Pacific Model), and the many students in the Mesoscale Air-Sea Interaciton Group who contributed.

REFERENCES

Anderson, D. L. T., and A. E. Gill, Spin-up of a stratified ocean, with application to upwelling, *Deep Sea Res.*, *22*, 583–596, 1975.

Battisti, D. S., and B. M. Hickey, Application of remote wind-forced coastal trapped wave theory to the Oregon and Washington coasts, *J. Phys. Oceanogr.*, *14*, 887–903, 1984.

Bjerknes, J., A possible response of the atmospheric Hadley circulation to equatorial anomalies in ocean temperature, *Tellus*, *18*, 820–829, 1966.

Chelton, D. B., and R. E. Davis, Monthly mean sea-level variability along the west coast of North America, *J. Phys. Oceanogr.*, *12*, 757–864, 1982.

Clarke, A. J., Observational and numerical evidence for wind-forced coastal trapped long waves, *J. Phys. Oceanogr.*, *7*, 231–247, 1977.

Clarke, A. J., The reflection of equatorial waves from oceanic boundaries, *J. Phys. Oceanogr.*, *13*, 1193–1207, 1983.

Emery, W. J., and K. Hamilton, Atmospheric forcing of interannual variability in the northeast Pacific Ocean: Connections with El Niño, *J. Geophys. Res.*, *90*, 857–868, 1985.

Enfield, D. B., and J. S. Allen, On the structure and dynamics of monthly mean sea level anomalies along the Pacific coast of North and South America, *J. Phys. Oceanogr.*, *10*, 557–578, 1980.

Gill, A. E., *Atmosphere-Ocean Dynamics*, edited by W. L. Donn, 662 pp., Academic, San Diego, Calif., 1982.

Gill, A. E., and E. H. Schumann, The generation of long shelf waves by the wind, *J. Phys. Oceanogr.*, *4*, 83–90, 1974.

Halliwell, G. R., and J. S. Allen, Large-scale sea level response to atmospheric forcing along the west coast of North America, summer 1984, *J. Phys. Oceanogr.*, *14*, 864–866, 1984.

Hickey, B. M., The California Current System—Hypothesis and facts, *Prog. Oceanography*, *8*, 191–279, 1979.

Huang, J. C. K., Response of the NCAR general circulation model to North Pacific sea surface temperature anomalies, *J. Atmos. Sci.*, *35*, 1164–1179, 1978.

Huyer, A., and R. L. Smith, The signature of El Niño off Oregon, 1982–1983, *J. Geophys. Res.*, *90*, 7133–7142, 1985.

Inoue, M. I., and J. J. O'Brien, Trends in sea level in the western and central equatorial Pacific during 1974–1975 to 1981, *J. Geophys. Res.*, *92*, 5045–5051, 1987.

Inoue, M. I., J. J. O'Brien, W. B. White, and S. E. Pazan, Interannual variability in the tropical Pacific for the period 1979–1982, *J. Geophys. Res.*, *92*, 11,671–11,679, 1987.

Kubota, M., and J. J. O'Brien, Variability of the upper tropical Pacific Ocean model, *J. Geophys. Res.*, *93*, 13,930–13,940, 1988.

Lagos, P., T. P. Mitchell, and J. M. Wallace, Remote forcing of sea surface temperature in the El Niño region, *J. Geophys. Res.*, *92*, 14,291–14,296, 1987.

McCreary, J. P., and D. L. Anderson, A simple model of El Niño and southern oscillation, *Mon. Weather Rev.*, *112*, 934–946, 1984.

Moore, D. W., Planetary-gravity waves in an equatorial ocean, Ph.D. dissertation, 207 pp., Harvard Univ., Cambridge, Mass., 1968.

Norton, J., D. McLain, R. Brainard, and D. Husby, *The 1982–1983 El Niño Event off Baja and Alta California and Its Ocean Climate Context, El Niño North*, edited by W. S. Wooster and D. L. Fluharty, 313 pp., Washington Sea Grant Program, University of Washington, Seattle, 1985.

Pan, Y. H., and A. H. Oort, Global climate variations connected with sea surface temperature anomalies in the eastern equatorial Pacific Ocean for the 1958–1973 period, *Mon. Weather Rev.*, *111*, 1244–1258, 1983.

Pares-Sierra, A., and J. J. O'Brien, The seasonal and interannual variability of the California Current system: A numerical model, *J. Geophys. Res.*, *94*, 3159–3180, 1989.

Quinn, W. H., V. T. Neal, and S. E. Antunez de Mayolo, El Niño occurences over the past four and a half centuries, *J. Geophys. Res.*, *92*, 14,449–14,462, 1987.

Rasmussen, E. M., and T. H. Carpenter, Variations in tropical sea surface temperature and surface wind fields associated with the Southern Oscillation/El Niño, *Mon. Weather Rev.*, *110*, 354–384, 1982.

Rasmussen, E. M., and J. M. Wallace, Meteorological aspects of the El Niño–Southern Oscillation, *Science*, *222*, 1195–1202, 1983.

Reid, J. L., Jr., R. S. Schwartzlose, and D. Brown, Direct measurements of a small surface eddy off northern Baja California, *J. Mar. Res.*, *67*, 2491–2497, 1963.

Rienecker, M. M., and C. N. K. Mooers, The 1982–1983 El Niño signal off northern California, *J. Geophys. Res.*, *91*, 6597–6608, 1986.

Simpson, J. J., Large-scale thermal anomalies in the California Current during the 1982–1983 El Niño, *Geophys. Res. Lett.*, *10*, 937–940, 1983.

Simpson, J. J., A simple model of the 1982–1983 California El Niño, *Geophys. Res. Lett.*, *11*, 243–246, 1984.

Spillane, M. C., D. B. Enfield, and J. S. Allen, Intraseasonal oscillations in sea level along the west coast of the Americas, *J. Phys. Oceanogr.*, *17*, 313–325, 1987.

Weare, B. C., A. R. Navato, and R. E. Newell, Empirical orthogonal analysis of Pacific sea surface temperatures, *J. Phys. Oceanogr.*, *6*, 671–678, 1976.

Wyrtki, K., Sea level fluctuations in the Pacific during the 1982–1983 El Niño, *Geophys. Res. Lett.*, *12*, 125–128, 1985*a*.

Wyrtki, K., Water displacements in the Pacific and the genesis of El Niño cycles, *J. Geophys. Res.*, *90*, 7129–7132, 1985*b*.

M. A. Johnson and J. J. O'Brien, Mesoscale Air-Sea Interaction Group, Florida State University, Tallahassee, FL 32306.

(Received March 28, 1989;
accepted November 28, 1989.)